The Plant Cell, Vol. 17, 2107–2122, July 2005, www.plantcell.org

Gene Expression Profiles of *Blumeria graminis* Indicate Dynamic Changes to Primary Metabolism during Development of an Obligate Biotrophic Pathogen [W]

Maike Both,[a] Michael Csukai,[b] Michael P.H. Stumpf,[c] and Pietro D. Spanu[a,1]

[a] Division of Biology, Imperial College London, London, SW7 2AZ, United Kingdom
[b] Syngenta, Jealott's Hill International Research Centre, Bracknell, Berkshire, RG42 6EY, United Kingdom
[c] Centre for Bioinformatics, Division of Molecular Biosciences, Imperial College London, London, SW7 2AZ, United Kingdom

cDNA microarrays of *Blumeria graminis* f sp *hordei* transcript profiles during the asexual development cycle reveal the dynamics of global gene expression as the fungus germinates, penetrates, feeds on its host, and produces masses of conidia for dispersal. The expression profiles of genes encoding enzymes involved in primary metabolism show that there is a striking degree of coordinate regulation of some of the genes in the same pathway. In one example, genes encoding several glycolytic enzymes are significantly upregulated as mature appressoria form and also in infected epidermis, which contain fungal haustoria. In another example, mRNAs for lipid degrading enzymes are initially expressed at high levels in the conidia and the early germination stages and decrease significantly later. We discuss these results and draw inferences on the metabolic status of this obligate biotrophic fungus as it infects its host and completes its life cycle.

INTRODUCTION

Blumeria graminis f sp *hordei* is an economically important pathogen of cereals that causes barley powdery mildew. Infected barley (*Hordeum vulgare*) shows the typical symptoms of white, powdery pustules and suffers as a result of the rerouting of its nutrients into the fungus, which proliferates and disperses very rapidly. Yield losses of up to 20% can occur (Czembor, 2002). Protection from this disease can be achieved using resistant crop cultivars or by spraying foliar fungicides.

B. graminis is an obligate biotrophic pathogen: it does not grow in axenic cultures and can only complete its life cycle on the living host. The asexual life cycle of *B. graminis* proceeds in a strictly programmed way and is highly synchronous (Both et al., 2005). The infection process (Figure 1) starts when wind-dispersed conidia come to rest on the surface of a barley leaf and immediately begin to produce an extracellular matrix, which probably serves to attach the fungus to the surface and also helps to obtain surface signal cues (Carver et al., 1999; Wright et al., 2002). A short primary germ tube appears within an hour of inoculation; the tube senses the nature of the surface on which the conidia germinate (Kinane et al., 2000; Nielsen et al., 2000). Shortly afterwards, a second germ tube emerges from the conidium. Its tip grows to form a swollen, hooked structure: the appressorium. This is clearly distinguishable at 8 h postinoculation (hpi). At 15 hpi, a penetration peg forms underneath the appressorium and breaks the plant cell wall by the combined action of high turgor pressure in the appressorium and enzymatic cell wall breakdown at the tip of the peg itself (Francis et al., 1996; Pryce-Jones et al., 1999). The peg does not breach the plant plasmalemma, and a haustorium develops in the periplasmatic space. Haustoria are the feeding structures of *B. graminis* that deliver nutrients from the plant and enable the fungus to proliferate rapidly on the surface of the leaf and produce epiphytic mycelium and additional secondary haustoria. After 3 d postinoculation (dpi), the fungal colony is visible to the naked eye on the leaf surface, and subsequently the colony begins to produce conidiophores, which generate a large number of conidia. These are airborne and can distribute the fungus to other host plants many miles away.

Biotrophic pathogens establish an intimate relationship with their host where the host cells remain alive while the metabolites are diverted to feed the pathogen. Many pathogenic fungi have at least a phase in which biotrophy is attained, and in some cases this lasts for nearly all the life cycle of the fungus. For others, an initial biotrophic phase is followed by a necrotrophic one in which the host cells are killed and the fungus feeds off the spoils of the dead plant cells. Much of what is known about biotrophic fungi and their metabolism has been studied on nonobligate biotrophs, such as *Cladosporium fulvum* (Thomma et al., 2005), *Magnaporthe grisea* (Talbot, 2003), and *Mycosphaerella graminicola* (Palmer and Skinner, 2002). Much less is known about the obligate biotrophs, such as rust fungi or the powdery mildews. These fungi attain an extraordinary level of biological compatibility with their host, and it is still unclear why their biotrophy is obligate. One possibility is that they have evolved so far down the

[1] To whom correspondence should be addressed. E-mail p.spanu@imperial.ac.uk; fax 44-20-75842056.
The author responsible for distribution of materials integral to the findings presented in this article in accordance with the policy described in the Instructions for Authors (www.plantcell.org) is: Pietro D. Spanu (p.spanu@imperial.ac.uk).
[W] Online version contains Web-only data.
Article, publication date, and citation information can be found at www.plantcell.org/cgi/doi/10.1105/tpc.105.032631.

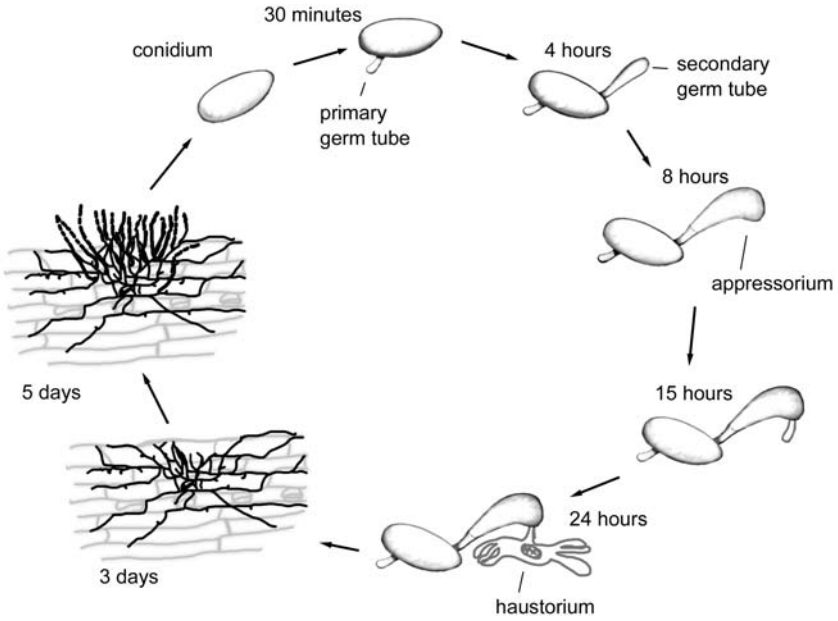

Figure 1. Asexual Life Cycle of *B. graminis* f sp *hordei*.

The prepenetration stages are those from ungerminated conidia up to the development of a functional appressorium (15 hpi) and a penetration peg initial. The postpenetration stages are those that follow the formation of a fully functional haustorium (24 hpi) and result in the development of hyphae on the surface of the leaf (epiphytic mycelia) that eventually produce abundant conidia 3 to 4 dpi. In these stages, fungal nutrition is supported by the activity of many secondary haustoria inside the plant epidermal cells.

route of compatibility with their host to lose some of the metabolic competence and are reliant on a plant for the supply of complex nutrients. A first indication that this might not be the case was the observation that *B. graminis* appears to have all the amino acid biosynthetic pathways of nonobligate fungi (Giles et al., 2003); however, it remains to be seen whether other fundamental primary metabolic pathways are present in obligate pathogens such as *B. graminis* and whether the genes encoding enzymes on these pathways are expressed and controlled in any way that is different from nonobligate pathogens.

The fact that *B. graminis* is an obligate biotroph limits the experiments that can be performed to understand the processes that underpin fungal development and cause disease. However, recent advances in high-throughput technologies, such as microarray studies, allow the simultaneous analysis of a large number of genes, and we have demonstrated that is possible to apply these techniques to *B. graminis* as it develops on its host plant (Both et al., 2005). Here, we describe the analysis of transcript expression profiles of genes that encode enzymes of *B. graminis* primary metabolism. These profiles enable us to analyze the dynamics of the expression of genes involved in metabolism and thus help to elucidate, on a large scale, the processes likely to contribute to the development in this fungus.

We identified correlation in expression patterns for several genes encoding enzymes on the pathways of the carbohydrate, lipid, and amino acid metabolism during development in planta; this correlation points to coordinate regulation of the glycolysis pathway, lipid degradation, glycogen breakdown, the Met pathway, and of several tRNA synthetases. From the results, we propose a model that describes the metabolic processes that are prevalent at different stages in the life cycle of *B. graminis*.

RESULTS

Microarray Design

The target DNA on the microarrays consisted of PCR products from three cDNA libraries, representing three different stages of development: ungerminated and germinated conidia (Thomas et al., 2001) and epiphytic mycelium (Eckert et al., 2001).

The probes were derived from six stages of the asexual development of *B. graminis* (Figure 1), and two of these time points were divided into an epiphytic and an in planta sample. Thus, sample RNA was isolated from the following: (1) fresh ungerminated conidia, collected directly from colonies on the plant; (2) germinated conidia 4 hpi, when a primary and an appressorial germ tube have developed; (3) germinated conidia 8 hpi, when the appressorium matures and generates turgor pressure as well as secretes enzymes for successful penetration; (4) germlings 15 hpi, when a haustorial bulb is developing inside the plant; (5) epiphytic mycelium 3 dpi, when the fungus is proliferating on the plant surface; (6) infected epidermis 3 dpi, containing the haustoria of the fungus; (7) epiphytic mycelium 5 dpi, when conidium production has begun; (8) infected epidermis 5 dpi, containing fungal haustoria. For each stage, three biological replicate samples were collected.

All Cy3-labeled cDNAs of these samples were cohybridized with a Cy5-labeled aliquot of a reference probe. The latter

was a pool from equal amounts of mRNA from all collected samples, representing the average gene expression amongst all conditions tested. This enabled us to make all samples comparable to each other as well as creating a signal for all target sequences that were represented in at least one of the probes. The ratio of signal intensity between sample (Cy3) versus reference (Cy5) was $\log_2$ transformed. We referred to this value as the relative expression index (REI). By plotting the averaged REI of each developmental stage in a graph (REI versus developmental stage), we created the expression profiles representing the developmental changes in transcript levels shown in this article.

Glycolysis

The arrays include cDNAs encoding enzymes that catalyze eight glycolysis reactions. The REI profiles for these cDNAs are shown in Figure 2. The expression profiles of fructose diphosphate aldolase, triose phosphate isomerase, glyceraldehydes phosphate dehydrogenase, phoshoglycerate kinase phoshoglucomutase, and pyruvate kinase exhibit a similar expression pattern: there was a significant increase in mRNA abundance after germination of the conidia, which peaked first at 8 hpi ($P < 10^{-6}$, apart from phosphoglycerate kinase where $P < 0.0005$, thus still significant after a Bonferroni correction; Sokal and Rohlf, 1981), decreased thereafter, and increased again significantly in the infected epidermis, most notably at 5 dpi ($P < 10^{-5}$, apart from phosphoglycerate kinase where $P < 0.001$; this is however still significant after Bonferroni correction). The expression profiles of hexokinase and enolase were clearly different: in both cases there was no evident variation in the levels of expression over time.

Pentose Phosphate Pathway

The REI profiles for cDNAs that encode four pentose phosphate pathway enzymes are shown in Figure 3. Transcript levels of glucose-6-phosphate dehydrogenase increased after germination, peaked at 8 hpi, and then returned to basal levels, whereas those of transketolase were low at all stages before penetration of the host (conidia to 15 hpi) and were significantly higher ($P < 10^{-10}$) at all postpenetrative stages. Phosphogluconate dehydrogenase and transaldolase expression varied somewhat during development, but the changes did not appear to follow a clear trend. Thus, there was no evident coordinate expression for any of these enzymes.

Glycogen Metabolism

Many cDNAs on the arrays were identified as encoding enzymes involved in the metabolism of glycogen: these were divided into enzymes that catalyze glycogen breakdown (glycogen debranching enzymes, glucoamylase, and α-glucosidase) or glycogen synthesis (glycogen branching enzyme). The expression profiles of these cDNAs are shown in Figure 4. The glycogen debranching enzyme cDNAs were grouped into two groups depending on their patterns of expression. Glycogen debranching enzyme I cDNAs were represented relatively highly in the prepenetration stages, and their levels dropped markedly in the stages after penetration (3 and 5 dpi) ($P < 10^{-8}$). Glycogen debranching enzyme II cDNAs also showed a lower expression level in the postpenetration stages compared with earlier time points, but the difference was not as pronounced, though still significant ($P < 10^{-6}$). Glucoamylase transcripts accumulated to higher levels immediately after germination of the conidia and remained high at all prepenetration stages. After the fungus penetrated the host, there was a strong reduction in transcript abundance, down to levels found in conidia. Expression profiles of α-glucosidase showed a less marked trend with a slight but significant ($P < 10^{-10}$) downregulation only in the later stages of infection in the infected epidermis. Conversely, the cDNA for a glycogen branching enzyme, the only target on the array that encoded an enzyme of glycogen synthesis, was expressed at low levels in all stages of development, with the exception of a significantly ($P < 10^{-8}$) high level in the epiphytic mycelium 5 dpi.

Lugol Stain

Lugol is a stain based on KI and I_2 that bind to glycogen, which is then visualized as a brown complex. We stained *B. graminis* as it developed on barley epidermis. Ungerminated conidia readily took up the stain and appeared deep brown (Figure 5A). Both primary and secondary appressorial germ tubes 6 hpi were yellow similar to that of the plant cell walls (Figure 5B). The intensity of the brown stain in the germinating conidium decreased steadily in the next few hours; 15 hpi the conidia that had germinated were less stained than ungerminated ones (Figure 5C, asterisk). The haustoria (Figure 5D, arrowhead) and the epiphytic hyphae (Figure 5F) were yellow at all times. In contrast with this, the conidiophores (including the foot cells; data not shown) and the developing conidia were dark brown (Figures 5E and 5F).

Lipid Degradation

There were many cDNAs encoding enzymes that catalyze degradation of lipids present on the microarrays (Figure 6). The most numerous were lipases: enzymes that hydrolyze fatty acids from triacylglycerol. We have grouped these lipases into four categories: the first three groups (I to III) (EC 3.1.1.3) on the basis of their patterns of expression and as monoglyceride lipase (EC 3.1.1.23) on the basis of the similarity to this class of enzymes. Group I lipase mRNAs were abundant in ungerminated conidia and germinating conidia 4 hpi, then decreased steadily and reached the lowest levels in infected epidermal cells 5 dpi. Group II lipase mRNAs remained at a constant level throughout development, with the exception of the infected epidermis samples, in which the levels were approximately eightfold lower. The group III lipase mRNAs and the monoglyceride lipase signals remained constant throughout the development. Four classes of cDNAs encoding enzymes that degrade fatty acids were identified in the arrays. Transcript abundance of these genes was high in the prepenetration stages (conidia to 15 hpi) and decreased in the epiphytic hyphae and most prominently in the

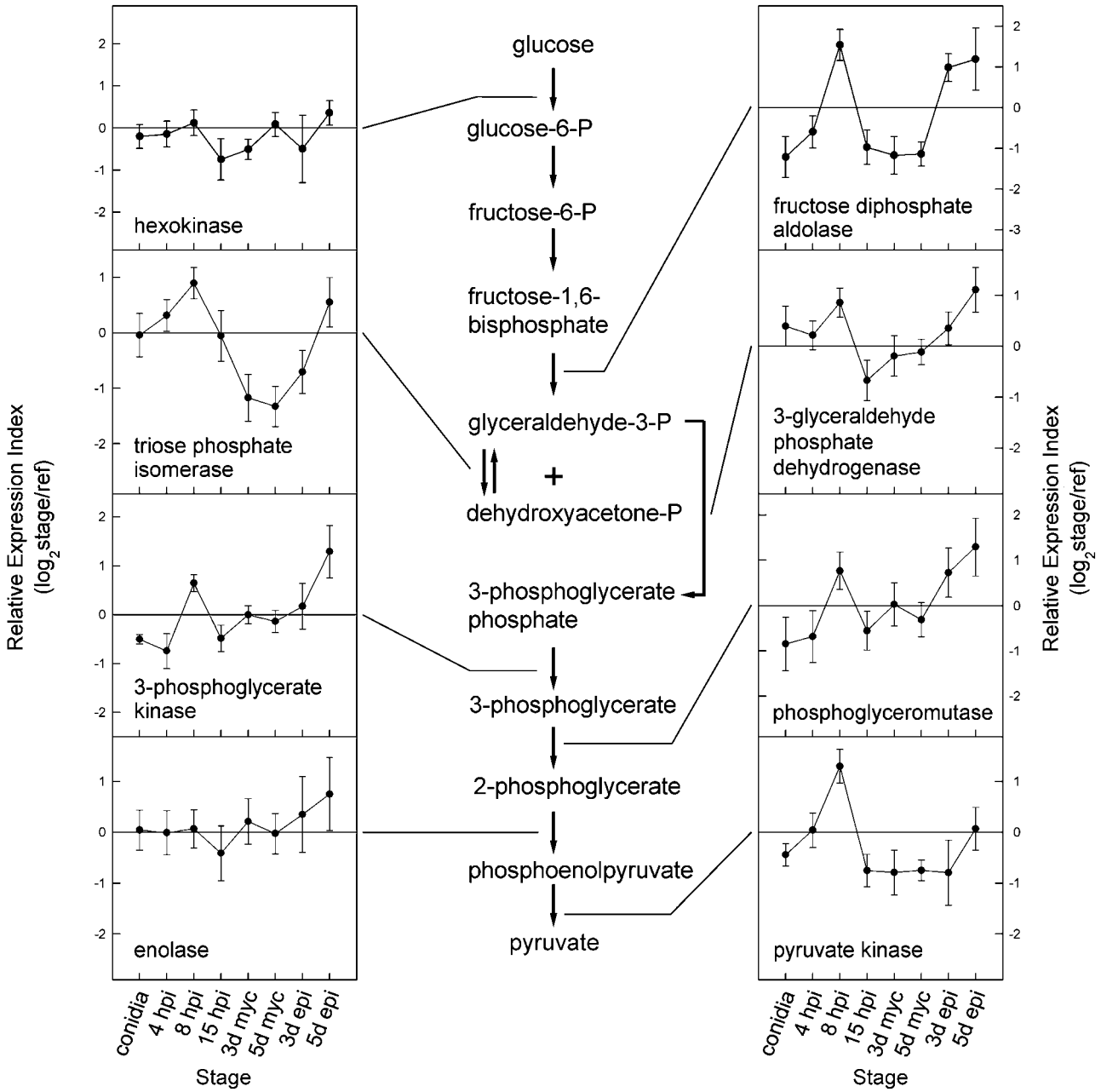

Figure 2. Expression Profiles of the RNAs Encoding Glycolytic Enzymes.

The REI of eight genes represented on the arrays is mapped onto a diagrammatic representation of glycolysis. REI of each cDNA is the $\log_2$ of the ratio between the signal derived from the hybridization with labeled cDNA from each stage and the reference probe. Each value represents the mean and standard deviation of three independent replicate experiments for each stage and all cDNAs on the arrays that encode the same enzyme.

infected epidermis samples. The most striking difference was observed for enoyl-CoA hydratase, which showed a 16-fold drop of mRNA levels between the 4 hpi samples and the epidermis cells containing haustoria 3 and 5 dpi. Thus, all four fatty acid degrading enzymes exhibited evident coregulation, which is also revealed by the branching pattern in the dendrogram (see below and Figure 9).

Nile Red Stain

We used Nile Red stain to visualize lipids in *B. graminis* (Figure 5). In the ungerminated conidia, numerous small intense yellow droplets were clearly visible over a background of diffuse bright orange fluorescence (Figure 5G). After germination, when the appressorial germ tube is formed, the yellow droplets disappeared

from the conidia, and the diffuse orange fluorescence decreased in intensity (Figure 5H). In Figure 5J, it is possible to compare the relative intensity of the orange fluorescence in an ungerminated conidium (asterisk) and a conidium 24 h after germination. At the same time, the appressorium acquired an intense diffuse orange fluorescence (Figure 5H). *B. graminis* colonies 24 hpi penetrated the barley epidermal cells and produced haustoria (Figure 5I, arrowhead). The haustoria were not fluorescent, but the external hyphae that grew on the surface of the leaf showed a diffuse orange fluorescence (Figure 5J). At 5 dpi, when *B. graminis* colonies were producing abundant conidia, the external hyphae fluoresced with a weak diffuse orange signal, but the conidiophores were much more intensely fluorescent, and bright yellow vesicles appeared in the nascent conidia (Figures 5K and 5L).

Met Metabolism

Five enzymes of the Met metabolic pathway were identified from the annotated cDNAs (Figure 7). mRNA levels of three

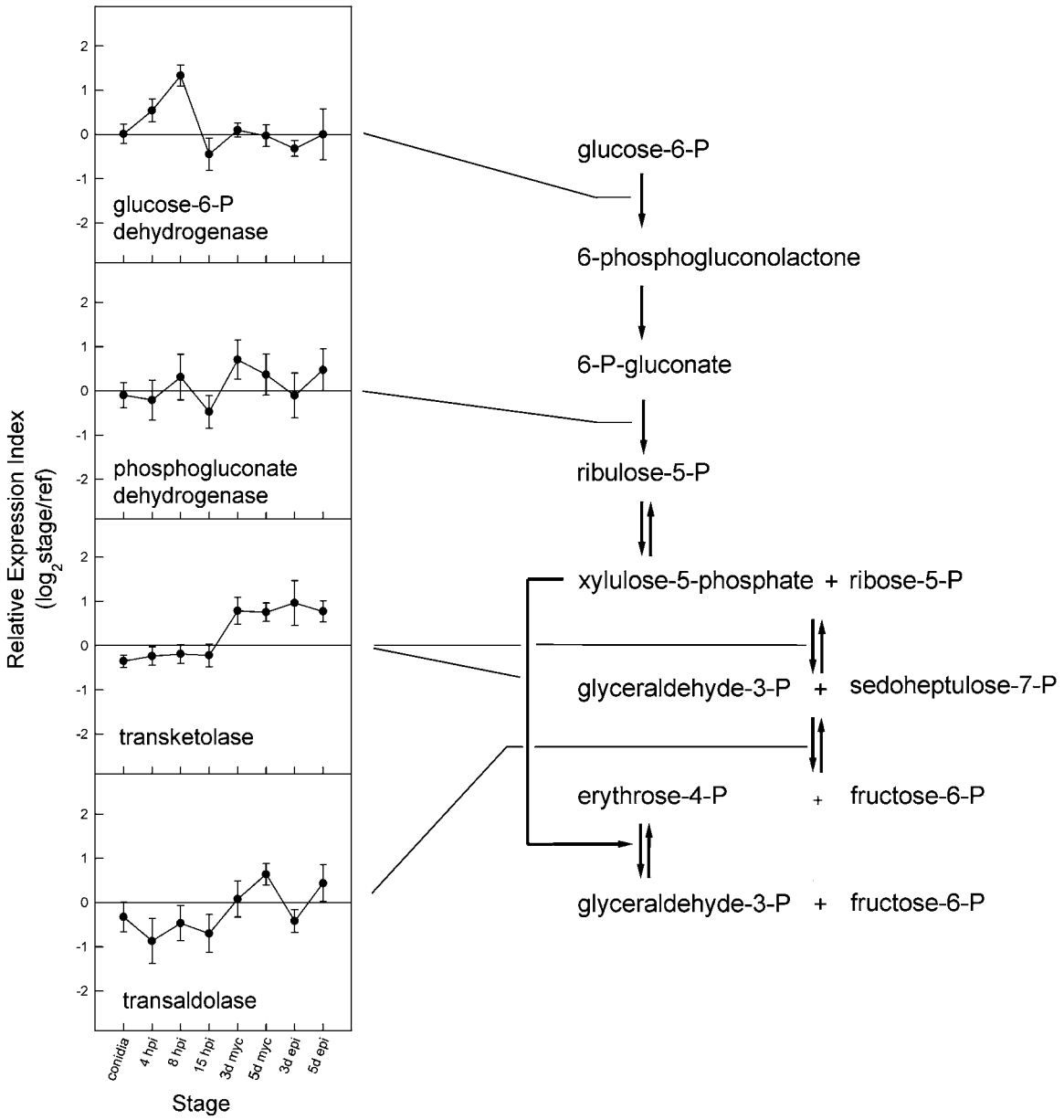

Figure 3. Expression Profiles of the RNAs Encoding Enzymes on the Pentose Phosphate Pathway.

The REI of the four genes represented on the arrays is mapped onto a diagrammatic representation of the pentose phosphate pathway. Each value represents the mean and standard deviation of three independent replicate experiments for each stage and all cDNAs on the arrays that encode the same enzyme.

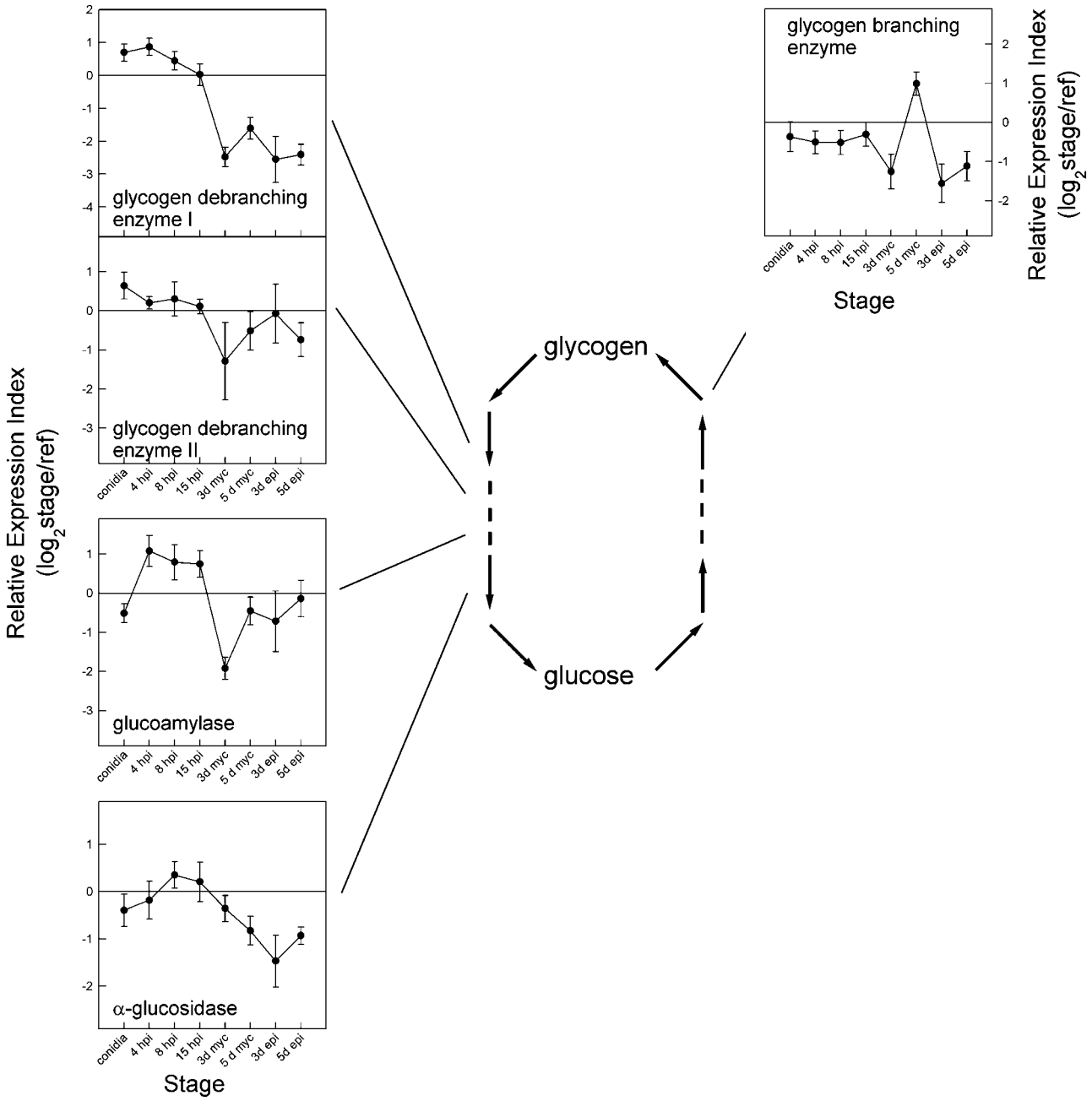

Figure 4. Expression Profiles of the RNAs Encoding Enzymes of Glycogen Metabolism.

The REI of the glycogen metabolism genes represented on the arrays is mapped onto a simplified representation of the glycogen synthesis (on the right) and glycogen breakdown (on the left). The expression profiles cDNAs encoding glycogen debranching enzymes identified two evident groups and are shown separately. Each value represents the mean and standard deviation of three independent replicate experiments for each stage and all cDNAs on the arrays that encode the same enzyme.

of the enzymes (adenosyl homocysteinase, Met synthetase, and adenosylmethionine synthase) were low in the prepenetration stages and rose sharply twofold to eightfold in the 3 and 5 dpi mycelium stages, with the level dropping fourfold to eightfold in the infected epidermis. Thus, these enzymes showed a striking correlation in their expression profiles (see also Figure 9). The expression profiles of homoserine acetyltransferase and cystathione γ-lyase were different: cystathione γ-lyase did not show a clear trend in its expression pattern, whereas mRNA levels of homoserine acetyltransferase increased in the samples from infected epidermis.

tRNA Synthases

The transcript profiles of all cDNAs annotated as tRNA synthases were grouped into three categories, depending on the trends in expression levels (Figure 8). Group I cDNAs (aspartyl-, arginyl-, and glutamyl-tRNA synthase) were relatively low in the prepenetration stages and increased twofold in all postpenetration stages. Group II cDNAs (phenylalanyl-, valyl-, and cysteinyl-tRNA synthase) did not share the same distinctive separation, but expression steadily increased during development. On the other hand, group III cDNAs (which included tyrosyl- and alanyl-tRNA synthase) were characterized by no significant variation of expression levels throughout development.

Hierarchical Cluster Dendrogram

All the REIs of the genes analyzed in this article were subjected to hierarchical cluster analysis (see supplemental data online). The

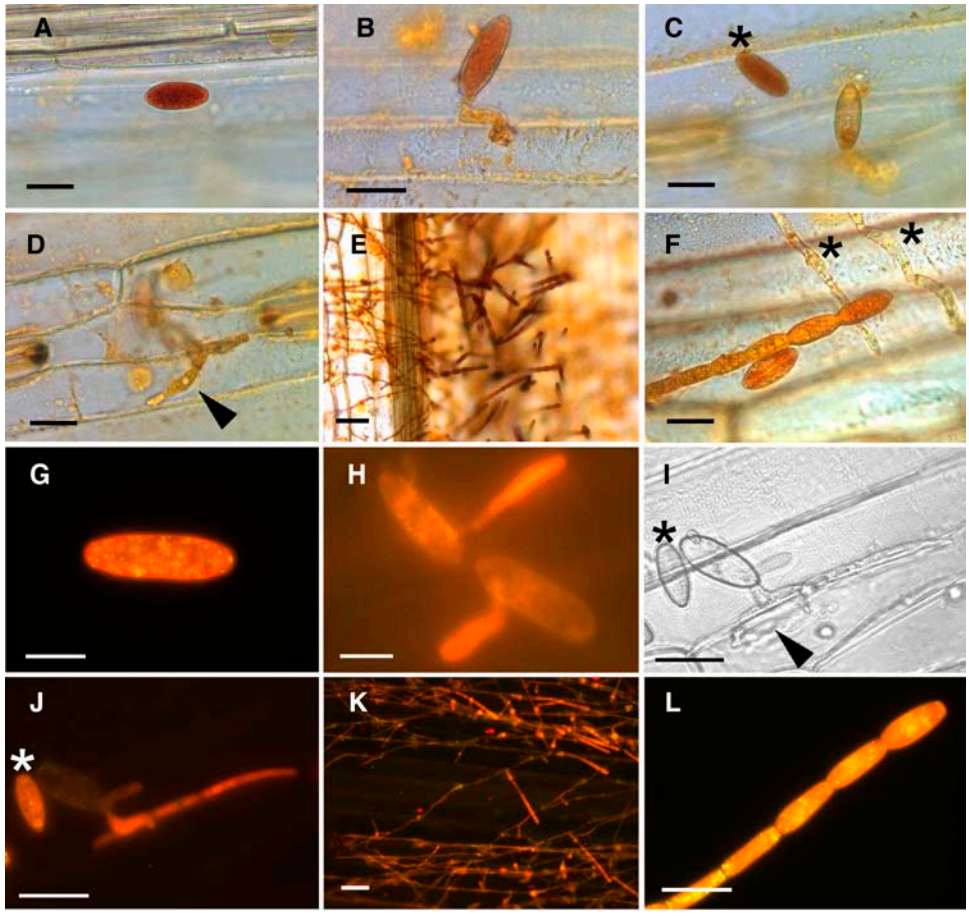

Figure 5. Lugol Staining of Glycogen and Nile Red Staining of Lipid Bodies in *B. graminis*.

Barley leaves were inoculated with *B. graminis* conidia. At given times the epidermis of the infected leaves was stripped and stained with Lugol solution (**[A]** to **[F]**) or with Nile Red (**[G]** to **[L]**) and observed by bright-field or epifluorescence microscopy.
(A) Ungerminated conidium. Bar = 10 μm.
(B) Conidia 6 hpi on the surface of a barley epidermal strip. Bar = 10 μm.
(C) Germinated conidium 15 hpi and an ungerminated conidium (asterisk) used as a control to reveal the decrease in yellow–brown. Bar = 10 μm.
(D) Colony 24 hpi showing a haustorium in its early stage of development (arrowhead). Bar = 10 μm.
(E) Mature colony 5 dpi at low magnification revealing an accumulation of brown stain in the mature conidiophores. Bar = 100 μm.
(F) Chain of newly formed conidia in a colony 5 dpi showing an accumulation of brown staining material compared with the yellow epiphytic hyphae (asterisks). Bar = 20 μm.
(G) Ungerminated conidium. Bar = 10 μm.
(H) Conidia 6 hpi on the surface of a barley epidermal strip. Bar = 10 μm.
(I) and **(J)** Bright-field image and epifluorescence, respectively, of a colony 24 hpi: an ungerminated conidium (asterisk) is visible near a colony with a newly developed haustorium (arrowhead). Bars = 10 μm.
(K) Epifluorescence image of a colony 5 dpi: at low magnification the relative fluorescence intensity of the epiphytic hyphae and the conidiophores is visible. Bar = 100 μm.
(L) Chain of newly formed conidia in a colony 5 dpi. Bar = 20 μm.

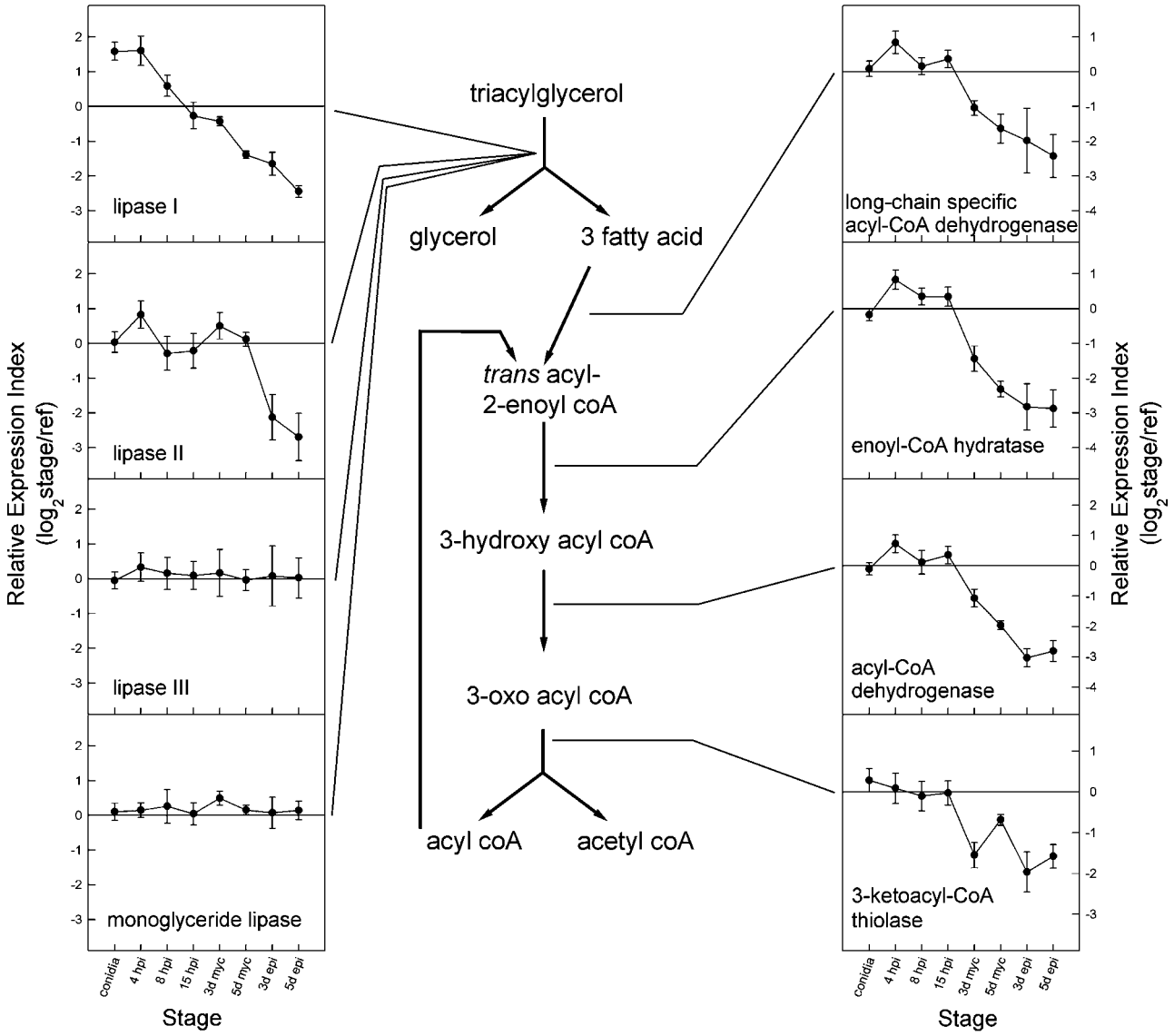

Figure 6. Expression Profiles of the RNAs Encoding Enzymes of Lipid Catabolism.

The REI of the lipid degradation genes represented on the arrays is mapped onto a simplified representation of the lipid breakdown pathway. Four groups of lipases (left) were identified because of the similarities in their REI profiles and because of the substrate specificity determined from the gene annotation. Four cDNAs encoding enzymes of the β-oxidation chain are shown at the right. Each value represents the mean and standard deviation of three independent replicate experiments for each stage and all cDNAs on the arrays that encode the same enzyme.

results were displayed as a dendrogram (Figure 9) showing the degree of similarity of the expression profiles of the various genes. Many of the expression profiles of genes that encode enzymes on related pathways appear to cluster together. For example, the glycolysis and pentose phosphate cycle genes, with the exception of transketolase, are on one branch of the tree; six out of the eight lipid degradation enzymes are very close clades, the two exceptions to this (lipase III and monoglyceraide lipase) are on completely different clades. The three enzymes that catalyze reactions on the *S*-adenosyl Met cycle (adenosyl homocysteinase, Met synthetase, and adenosylmethionine synthase) are on the same branch, whereas the other two enzymes in Met metabolism (homoserine acetyltransferase and cystathione γ-lyase) appeared on separate clades. Of the eight tRNA synthetase genes, six are on the same branch and only two (tyrosyl-tRNA synthetase and alanyl-tRNA synthetase) are removed. The main exception to this trend of clustering within biochemically related pathways is the group of glycogen biosynthesis genes, where members of this pathway are distributed throughout the branches of the dendrogram.

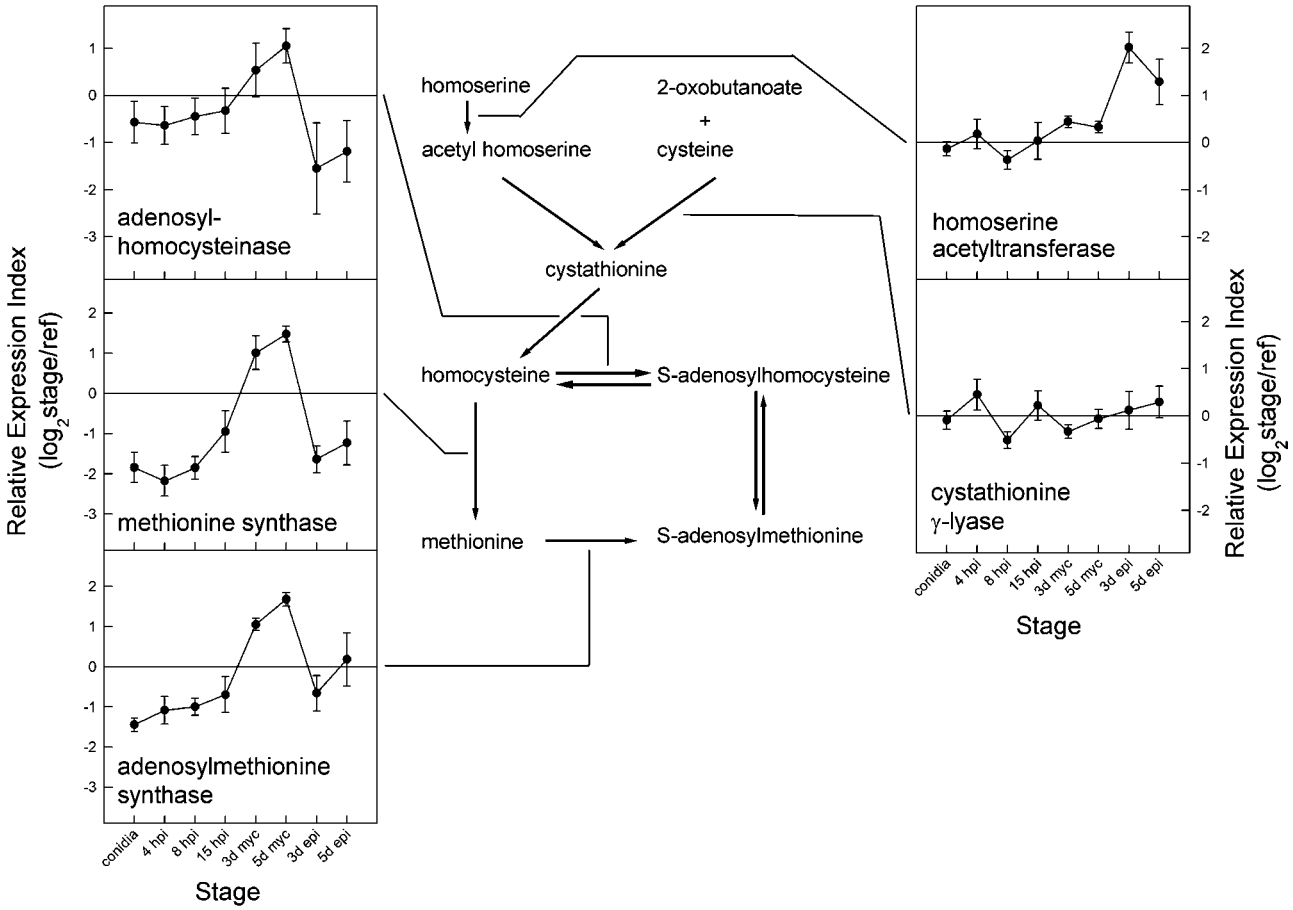

Figure 7. Expression Profiles of the RNAs Encoding Enzymes of Met Metabolism.

The REI of the Met metabolism genes represented on the arrays is mapped onto a representation of the pathways of Met metabolism. Three enzymes that are involved in the cycle of active methyl groups are shown on the left. Two other genes encoding enzymes on the pathway of Met synthesis are shown on the right. Each value represents the mean and standard deviation of three independent replicate experiments for each stage and all cDNAs on the arrays that encode the same enzyme.

DISCUSSION

In this article, we analyzed the results from microarray experiments that measured the abundance of mRNAs encoding enzymes involved in primary metabolism of the plant pathogenic fungus *B. graminis*. In this study, we investigated the complete asexual life cycle of an obligate biotroph on its host. In particular, we probed four stages of development that precede penetration: ungerminated conidia, germinated conidia, maturation of the appressorium, and penetration of the leaf epidermal cells. We also analyzed four stages after penetration: the mycelium collected 3 dpi that proliferates on the surface of the epidermis before sporulation, the epiphytic mycelium 5 dpi that is producing abundant asexual conidia, and the infected epidermis that contains the haustoria, 3 and 5 dpi. The latter two samples contain material from the host plant as well as the fungus; we have previously found that the plant material does not interfere significantly with the hybridization signals specific to fungal targets (Both et al., 2005).

The cDNA arrays included 2027 unigenes (Both et al., 2005), which we estimate to be approximately one-quarter to one-sixth of the expected number of genes in a filamentous fungus. The genes represented were likely to be those that are most actively expressed in the stages from which the libraries were originally made: germinated and ungerminated conidia (Thomas et al., 2001) and nonsporulating epiphytic mycelium (Eckert et al., 2001). Because the libraries were redundant, some genes were represented by more than one cDNA on the array. The data from these points were combined and increased the reliability of our expression analysis. Although the coverage of genes involved in primary metabolism was not complete, for some pathways cDNAs of more than half of the enzymes were represented on our arrays. We calculated the REI for each of the cDNAs on the array: the REI is a measure of the abundance of the mRNA at each stage relative to the average of all measurements throughout the eight stages investigated in this work (Both et al., 2005). The expression profiles for each gene were mapped to the metabolic pathways in the KEGG Pathway Database (Kanehisa et al., 2004).

We then analyzed the REI profiles in any one pathway to identify evident common trends in expression. Those members of genes from each pathway that show coregulation might share common *cis*- and *trans*-elements involved in their control. We report here some of the most evident examples of coexpression of the genes in common metabolic networks: glycolysis, glycogen metabolism, lipid degradation, Met metabolism, and synthesis of tRNAs.

Glycolysis is a central metabolic process in all organisms and was one of the pathways that is best represented in our microarrays: the cDNAs corresponding to 8 out of 10 enzymes central to glycolysis were on the arrays. There was a clear modulation of the mRNA levels of six out of the eight glycolytic genes analyzed, and the trends in expression followed very similar patterns. It is notable that the expression profiles of all of the genes encoding glycolytic enzymes appeared to cluster together on the same branch of the dendrogram represented in Figure 9. They showed a definite increase in activity during formation of the appressoria and the intracellular feeding structures, especially 5 dpi. These are likely to be the stages at which greater energy supply is required, first of all to generate turgor pressure in the appressorium to penetrate the plant cell walls; then, after penetration, there is a need to fuel proliferation of the external mycelium and production of masses of conidia. According to our data, it appears that in *B. graminis* this fuel is at least in part derived from the degradation of glucose through glycolysis. The results are in accordance with the observation that glucose is the predominant source of carbon that is taken up by haustoria of powdery mildews (Clark and Hall, 1998; Sutton et al., 1999). Two exceptions to this coordinated pattern of expression were hexokinase and enolase. These enzymes seem uncoupled from the coordinate regulation of the other glycolysis genes. There are reports of other instances in which only a subset of the genes of a given pathway is coregulated: for example, in yeast 24 out of 46 genes in glycolysis showed a correlated pattern of expression (Ihmels et al., 2004). Hexokinase is responsible for the phosphorylation of glucose. The fact that during formation of

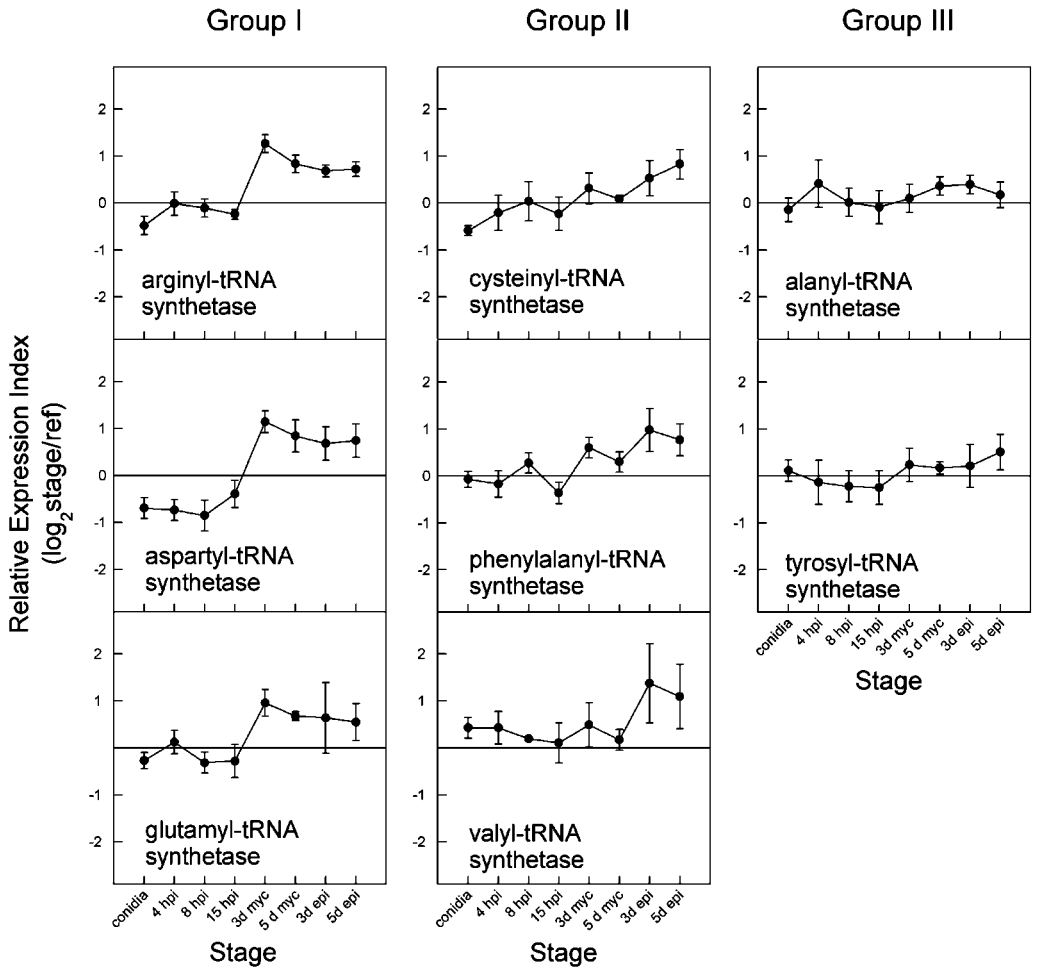

Figure 8. Expression Profiles of RNAs Encoding tRNA Synthases.

The REI of all eight tRNA synthases represented on the arrays are shown here. The tRNA synthase cDNAs are grouped into three classes based on the REI profiles. Each value represents the mean and standard deviation of three independent replicate experiments for each stage and all cDNAs on the arrays that encode the same enzyme.

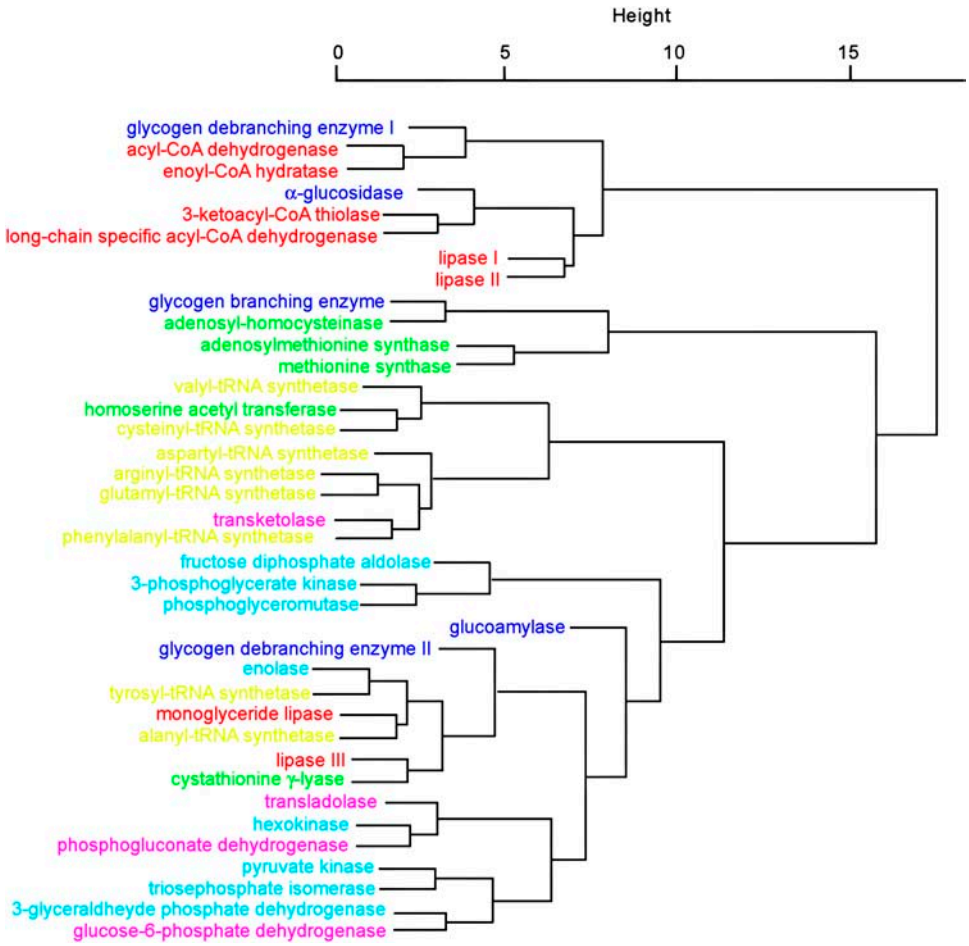

Figure 9. Hierarchical Cluster Dendrogram of the REI Profiles.

The tree represents a cluster analysis of the transcriptional profiles of the genes encoding enzymes on the primary metabolic pathways discussed in this article. The distance measure used was the standard Manhattan distance (see supplemental data online for details). The enzymes are color coded to show involvement on related pathways: glycolysis, turquoise; pentose phosphate pathway, purple; glycogen metabolism, blue; lipid degradation, red; Met metabolism, green; tRNA synthetases, yellow.

appressoria there was no evident significant increase in the hexokinase mRNA might suggest that phosphorylated glucose is derived directly from glycogen. Support for this hypothesis comes from evidence of increased glycogen degrading activity at this stage (see below).

Interestingly, the expression profile of fructose diphosphate aldolase is in marked contrast with the profile observed for that of fructose-1,6-bisphosphatase, where the levels of activity were constantly high in all prepenetrative stages and then dropped dramatically in all stages after penetration (Both et al., 2005). This difference in expression profile coincides with the fact that fructose-1,6-bisphosphatase catalyzes a reaction in the opposite direction of the major carbon flow thought to take place in glycolysis.

The pentose phosphate pathway plays a dual role in fungi in providing intermediates for gluconeogenesis and generating NADPH in the extramitochondrial cytoplasm (Jennings, 1995). In contrast with the evident coregulation of the majority of the glycolytic genes, the four cDNAs that encode enzymes in the pentose phosphate pathway did not show coordinate trends in expression, in spite of the fact that there was clear evidence of modulation of expression for glucose-6-phosphate and transketolase. Indeed, the mRNA levels of glucose-6P-dehydrogenase increased significantly during appressorium development, and the expression profile clustered with those of 3-glyceraldehyde phosphate dehydrogenase, triosephosphate isomerase, and pyruvate kinase. Expression levels of transketolase were relatively higher in all postpenetrative stages. This might result in a greater supply of sugars via gluconeogenesis; however, the same was not reflected by changes in the levels of transaldolase, an enzyme that catalyzes related reactions in this pathway. The observed absence of a regulatory cluster showed that the pathway was not a biologically linear metabolic flux, but rather a crossroads of different linear modules of the metabolism (Ihmels et al., 2004). In this respect, it must be noted that phosphofructokinase, considered as one of the key regulators of

glycolysis, is absent from our cDNA microarray and has not been identified yet in the published ESTs of Blumeria. Although no firm comment can be made by the absence of a gene from a study that does not cover the whole of the gene set, the obligate aerobic yeast Rhodotorula does not appear to possess this enzyme, and carbon is funneled into glycolysis via glucose-6-phosohate and the gluconeogenesis pathway (Jennings, 1995). Thus, the coexpression of glucose-6-phosphate dehydrogenase and some of the glycolytic enzymes observed here might support a similar scenario in Blumeria; however, a firm statement to this intent will require either the identification of phosphofructokinase or confirmation of its absence when the whole genome of Blumeria is sequenced.

Glycogen and lipids are two storage compounds that fungi accumulate in their conidia as has been recently shown in the rice pathogen *M. grisea* (Thines et al., 2000; Weber et al., 2001), *Colletotrichum lagenarium* (Tsuji et al., 2003), and the rust *Puccinia distincta* (Weber and Davoli, 2002). On our microarrays, four cDNAs encoded enzymes that catalyze reactions involved in glycogen metabolism. The expression of three genes implicated in glycogen breakdown was relatively high in the conidia or immediately after germination. These levels then decreased significantly after penetration. These results agree with earlier evidence that the glycogen debranching enzyme transcript is increasingly abundant during germination (Thomas et al., 2002). Conversely, the only cDNA on the array involved in glycogen synthesis showed a peak of activity in the epiphytic mycelium 5 dpi: the stage that is characterized by massive production of conidia from epiphytic conidiophores. We used the Lugol stain, based on KI/I_2, to visualize glycogen during development. Lugol forms a brown complex with glycogen that is readily visible under the microscope and is distinguishable from the yellow complex formed with the walls of both Blumeria and the barley cells. The imaging of the dark brown Lugol complex throughout asexual development revealed that glycogen is present in conidia before germination; this then decreases after the primary and secondary appressorial germ tubes are formed. We did not observe any prominent brown complex in the germ tubes, the appressoria, the haustoria, or the epiphytic hyphae that grow over the surface of the infected plant. A similar study performed on *M. grisea* (Thines et al., 2000) indicated that in that fungus conidia also contain glycogen that is degraded after germination. The *M. grisea* appressoria becomes transiently stained with the KI/I_2, and the label then disappears. This is in contrast with our observations in Blumeria, where we did not observe this transient staining of the appressoria. Note that we did not observe any peak in the expression of glycogen biosynthetic genes in the prepenetration stages either. This suggests that although in broad terms the processes that support the formation and functioning of appressoria in Blumeria and Magnaporthe are similar, there are subtle differences in the dynamics of metabolism between the two fungi. Taken together, this data indicate that conidia contained glycogen as a storage product, a source of carbon and energy to drive biosynthesis of new structures and function before penetration. When conidia were formed (5 dpi), glycogen was actively synthesized and accumulated in the propagules, most likely using glucose assimilated from the plant epidermal cells by the haustoria (Clark and Hall, 1998; Sutton et al., 1999).

The enzymes involved in lipid breakdown were represented on the arrays by numerous lipases that catalyze the severance of the bond between glycerol and fatty acids and by four enzymes that catalyze the breakdown of fatty acids themselves in the β-oxidation chain. The lipases were observed to group into four categories, depending on their overall expression and enzyme specificity. The first two classes and the four cDNAs encoding fatty acid degradation all had relatively high activities in the early, prepenetration stages and then diminished, most markedly, in the infected epidermal cells. These results hinted at a heightened lipid breakdown in the conidia and early germlings and a reduction in this capacity at later stages. Unlike the case of glycogen synthase, none of the cDNAs encoding lipid biosynthesis investigated here reveal any specific increase in mRNA accumulation in the assimilatory stages (data not shown). Thus, although the results did indicate that lipid is likely to be used up as a source of energy after germination, we have no direct evidence from the microarrays that lipid biosynthesis increased during formation of the conidia 5 dpi. This interpretation is also consistent with observations made in other plant pathogenic fungi: the activity of the isocitrate lyase promoter (from *Neurospora crassa*) fused to green fluorescent protein is high in the prepenetration epiphytic stages of infection in both *Tapesia yallundae* (Bowyer et al., 2000) and *M. graminicola* (Rohel et al., 2001) and decreases significantly after penetration of the cereal hosts; the absence of an isocitrate lyase cDNA on our microarrays prevents us from making a direct comparison with this data, and thus it remains to be seen whether Blumeria isocitrate lyase is also expressed in this manner.

To obtain further corroboration of the validity of our microarray results, we stained lipids with Nile Red to visualize their distribution. Neutral lipids stained with Nile Red fluoresce yellow (maximal emission at 590 nm) and polar lipids fluoresce orange (maximal emission at 600 nm) (Klinkner et al., 1997). Our data suggest that neutral lipid droplets are abundant in ungerminated conidia: this confirmed early observations of lipid bodies in *B. graminis* conidia (McKeen, 1970). Similar structures were observed in *Botrytis cinerea* and were referred to as spherosomes because of their acid phosphatase activity (Weber et al., 1999). In our studies, the lipid droplets disappeared from the conidia when the appressorial germ tube formed. This might point to the fact that the neutral lipid reserves were degraded and that polar lipids, possibly formed by lipase catalyzed breakdown of the neutral lipids, moved into the developing appressorium. This is similar to *M. grisea*, where lipid droplets move from the conidia into the appressorium, enlarge, and finally coalesce and are taken up into the vacuoles where lipid degradation occurs during appressorium maturation (Thines et al., 2000). It is interesting to note that in *M. grisea* the translocation of lipid droplets into the hyphal germ tube tip is linked to the MAP kinase PMK1 and that the protein kinase cPKA is required for lipolysis during formation of appressoria and turgor generation (Thines et al., 2000). We have recently found that *B. graminis* homologs of cPKA and of an upstream regulator of PMK1 are upregulated specifically during formation of *B. graminis* appressoria (Both et al., 2005).

There was no visible accumulation of lipids in the haustoria, and this may reflect the assimilatory function of this organ. At later stages, when new conidia were formed, polar lipids accumulated

in the conidiophores and eventually the yellow droplets of neutral lipids appear in the developing conidia. These cytochemical observations support the interpretation of the microarray analysis (i.e., that *B. graminis* uses lipids stored in conidia to drive colonization of the host plant); the lipids are first gradually hydrolyzed to generate energy for appressorial function (penetration) and eventually regenerated in the epiphytic mycelium when new conidia are formed.

We found no obvious patterns of coregulation of gene expression amongst the amino acid metabolic pathways with the exception of the Met biosynthesis pathway, shown in Figure 7. Highly coordinate expression was confined to the part of the pathway that forms the cycle involved in transfer of methyl groups. The cDNAs for three out of the four enzymes in this cycle were present in the libraries. This cycle serves to replenish the methyl group donors for methylation of nucleic acids, proteins, and various other small metabolites. In the green plant Lemna, the synthesis of the methyl donor adenosylmethionine accounts for 80% of the Met metabolism, and only 20% are used for protein synthesis (Giovanelli et al., 1985). According to the expression profiles, the cycle is particularly active in the epiphytic mycelium, reflecting the importance of methylation processes during this stage of development. This might mirror the high levels of proliferation and biomass production (e.g., methylation of DNA, synthesis and modification of proteins, and synthesis of lipids) that occurs in this phase of the life cycle. It might also contribute to the observed requirement for Met in *M. grisea* pathogenesis (Balhadere et al., 1999) and the expression of Met synthase during *C. fulvum* infection of tomato (*Lycopersicon esculentum*; Solomon et al., 2000). The expression of homoserine acetyltransferase and cystathione γ-lyase did not correlate with these three profiles, indicating that Met production and methylation were not linked but formed separate branches in the Met biosynthesis pathway.

The expression profiles of tRNA synthases in groups I and II (six out of eight enzymes identified in the libraries) demonstrate that mRNA abundance of these enzymes increases steadily during the development, particularly in the postpenetration stages. Although the average rise of mRNA levels may be slight, it is reflected in most of the profiles, and was therefore significant. This coincides with a similarly subtle but highly reproducible increase in expression found in profiles of protein synthesis genes during the 3- and 5-dpi mycelial stages (Both et al., 2005). Increased activity of tRNA synthases might thus help to feed the increased need for protein synthesis of proliferating stages, both the mycelium and the infected epidermis samples.

Microarrays measure the relative steady state mRNA abundance in a given sample. The analysis and interpretation of the results are based on two assumptions: first, a high level of mRNA compared with the baseline reference sample implies that there is a high level of resultant protein. Second, the high level of protein reflects an increase in overall activity of the corresponding enzymes. Posttranscriptional processing of mRNA and protein levels is not identified by microarrays; hence, interpretation of the data could potentially lead to false conclusions. However, the power of microarrays lies in their ability to analyze changes in mRNA levels for thousands of genes simultaneously, and we believe that at present, transcriptome analysis of Blumeria is a useful tool to undertake a large-scale study of its metabolism. The results of this study form the basis for new hypotheses and ideas for further investigation, but a complete validation of the hypothesis presented here concerning trends in metabolism during Blumeria infection will have to wait for the development of large-scale metabolomic studies in this fungus. A full list of all ESTs, their annotations, and their expression values are now publicly available (http://cogeme.ex.ac.uk/blumeria/blumeria_microarray.xls) so that the community can gather valuable information beyond the scope of this article.

In conclusion, the data from our microarrays showed a dynamic regulation of the genes involved in primary metabolism of the obligate biotrophic pathogen *B. graminis*. This regulation resulted in some striking instances of coexpression of genes in related metabolic pathways and antiregulated expression of pathways that flow in opposing directions. The inferred shifts in metabolism during the development and pathogenicity are summarized in Figure 10. *B. graminis* conidia use lipids and glycogen as energy

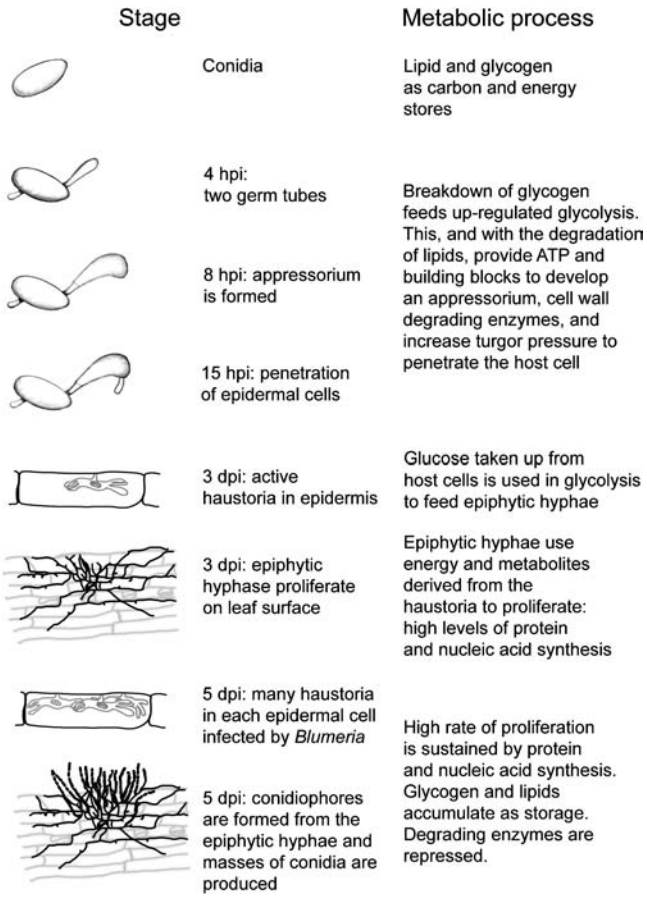

Figure 10. Model of the Changes in Metabolism That Occur in *B. graminis* during Development and Infection.

On the left is a diagrammatic representation and a description of the stages probed in this work; on the right is a summary of the most prominent changes in metabolism as deduced from coordinated shifts in the expression patterns of genes encoding key metabolic steps.

and carbon stores. As the germ tubes grow, these stores are broken down and carbon flows through an increasingly active glycolysis. The energy released and the building blocks formed are used to produce an active appressorium and drive the penetration of the plant cell wall. Once the haustoria are in place, the nutrients derived from the plant are channeled through glycolysis to support protein and DNA synthesis for the proliferation of the external hyphae and formation of masses of conidia in which glycogen is laid down as storage.

Although *B. graminis* is an obligate parasite, it appears to have all of the main metabolic pathways of filamentous fungi (Thomas et al., 2001, 2002; Soanes et al., 2002; Giles et al., 2003), and unlike many intracellular obligate parasites or bacteria (Andersson and Kurland, 1998; Andersson et al., 1998; Andersson and Andersson, 1999; Frank et al., 2002; Gardner et al., 2002; Cummings et al., 2004), it has not lost metabolic capacity nor has it lost the ability to modulate its metabolism. The question remains as to why *B. graminis*, like all the other powdery mildews and rusts, is an obligate pathogen. One possibility is that these fungi have acquired the competence to regulate their metabolic genes in response to signals from the host plants. In the absence of these signals, metabolic genes are expressed incorrectly (or not at all), and the fungi are thus unable to grow and multiply on complete but artificial growth substrates. It remains to be seen whether there will be any experimental evidence to corroborate this hypothesis and, if so, what the host-derived signals might be.

METHODS

Growth Conditions of Plants and Fungi

Barley (*Hordeum vulgare*) plants were grown from seed in an climate-controlled growth room at 17°C, with a 16-h-light/8-h-dark cycle. Plants were inoculated after 8 to 14 d by dusting fresh Blumeria conidia (race IM82) (Chaure et al., 2000) from already infected plants. The infected plants were kept in a greenhouse with supplemented light conditions (16 h). Twenty-four hours before every inoculation, the plants used to obtain the inoculum were shaken to remove old conidia and to achieve a consistent germination rate.

Construction of Blumeria Microarrays

The libraries were kept as bacteria or plasmid stocks at −80°C. Each clone was PCR amplified, with a primer modified with an amino group and C12 on the 5′ end. The products were concentrated by ethanol precipitation (Sambrook et al., 1987) and eluted in Genpak spotting buffer (Genetix, Hampshire, UK) to reach a final concentration of ~0.5 to 1 μg. DNA was spotted onto aminosilane-coated glass slides with an Omnigrid microarray spotter (GeneMachines, San Carlos, CA). Cross-linking of the DNA was achieved by incubating the spotted slides at 60°C for 3 h and at 100°C for 10 min. Slides were stored in the dark at room temperature.

RNA Extraction

Conidia were collected with a vacuum pump from colonies of infected plants. All other prepenetration stages and the epiphytic mycelium stages were collected by immersing the infected leaf into cellulose acetate (5%) dissolved in anhydrous acetone, letting the acetone evaporate, and collecting the fungal material that remained embedded in the cellulose acetate. This procedure is likely to ensure that all epiphytic fungal material is effectively dehydrated within a very short time from harvesting and, thus, that changes in transcript abundance as a result of the manipulation are minimized. Infected epidermis was collected as an epidermis peel after the epiphytic material had been removed. Total RNA was isolated using guanidine isothiocyanate (Chomczynsky and Sacchi, 1987), except for the epidermis samples, which were treated as described by the Qiagen RNeasy extraction kit (Crawley, UK). The total RNA from conidia was additionally dialyzed on 0.025 μm nitrocellulose (Millipore, Billerica, MA) filters over diethyl pyrocarbonate–treated water.

Probe Preparation and Microarray Hybridization

mRNA was converted into double-stranded cDNA using a primer with oligo(dT) and T7 promoter sequence and SuperScript II reverse transcriptase (Invitrogen, Carlsbad, CA). This was amplified by producing more mRNA with the MEGAscript T7 RNA synthesis kit (Ambion, Austin, TX). A second reverse transcription step with random primers and direct incorporation of Cy3 (sample) or Cy5 (reference) dUTPs (Amersham, Buckinghamshire, UK) yielded the fluorescent probes. Samples and reference probes were mixed, vacuum dried, and resuspended in hybridization buffer (50% deionized formamide, 6× SSC [1× SSC is 0.15 M NaCl and 0.015 M sodium citrate], 0.5% SDS, and 5× Denhardt's solution [1× Denhardt's solution is 0.02% Ficoll, 0.02% polyvinylpyrrolidone, and 0.02% BSA]). Hybridization was performed on prehybridized slides (6× SSC, 0.5% SDS, and 1% BSA for 1 h) for at least 16 h.

Microarray Data Normalization

The hybridization signal was detected with a Genepix 4000b dual laser scanner (AXON Instruments, Foster City, CA) and quantified with its software (GenePixPro3). The output files were normalized with Expressionist Refiner 3.1.6 (Genedata, Basel, Switzerland) using the functions background correction, Lowess correction, and unsupervised masking. The ratios between the Cy3 and C5 signals were $\log_2$ transformed for further data analysis.

Microarray Data Metabolic Analysis

The annotated libraries were screened to search for cDNAs that encode proteins with similarities to enzymes on the primary metabolic pathways in the KEGG database (http://www.genome.ad.jp/kegg/pathway.html). Their expression profiles were then compared, and groups of cDNAs encoding the same genes that showed evident coordinate profiles were grouped together. The REI values over the developmental time course were averaged, the standard deviation calculated, and displayed as a graph. The graphs were displayed on the KEGG pathway maps and related to the individual reactions catalyzed. These maps were then examined to identify trends in profiles of genes whose expression was coregulated.

Lugol and Nile Red Stains

B. graminis conidia or *B. graminis*–infected barley epidermis were placed on microscope slides and stained with Lugol reagent (KI/I_2; Chroma Gesellschaft, Münster, Germany) and 0.1% Triton X-100 and observed immediately or with Nile Red (2.5 μg/mL Nile Red in 50 mM Tris/maleate buffer, pH 5.2, 20 mg/mL polyvinylpyrrolidone, and 1% Triton X-100) following the protocol modified from Thines et al. (2000). The samples were viewed in bright field or epifluorescence with a Zeiss Axioscop 2 microscope (Jena, Germany) fitted with a 50W HBO mercury lamp and filter (BP485/20, FT510, LP 515).

Statistical Analysis

Differential gene expression was assessed using the nonparametric Wilcox test. Correlations, where reported, used Kendall's rank order statistic. In each case, a Bonferroni correction was applied to account for multiple comparisons; unless explicitly stated otherwise, P values are significant at the 1% level.

A hierarchical clustering procedure was used to test for coexpression. Simple Euclidean and Manhattan distances gave good agreement about the branching patterns. Details of the statistical analysis are given in the supplemental data online.

Sequence data from this article have been deposited with the EMBL/GenBank data libraries.

ACKNOWLEDGMENTS

This work was funded by a Biotechnology and Biological Science Research Council CASE studentship and by Syngenta. We are grateful to James Abbot and Sarah Butcher (Imperial College London) for advice and guidance on annotation of the EST database and to Adam Cleaver and Alan Evans (Syngenta) for assistance with the Expressionist software.

Received March 14, 2005; revised April 27, 2005; accepted May 13, 2005; published June 10, 2005.

REFERENCES

Andersson, J.O., and Andersson, S.G.E. (1999). Insights into the evolutionary process of genome degradation. Curr. Opin. Genet. Dev. **9,** 664–671.

Andersson, S.G.E., and Kurland, C.G. (1998). Reductive evolution of resident genomes. Trends Microbiol. **6,** 263–268.

Andersson, S.G.E., Zomorodipour, A., Andersson, J.O., Sicheritz-Ponten, T., Alsmark, U.C.M., Podowski, R.M., Naslund, A.K., Eriksson, A.S., Winkler, H.H., and Kurland, C.G. (1998). The genome sequence of Rickettsia prowazekii and the origin of mitochondria. Nature **396,** 133–140.

Balhadere, P.V., Foster, A.J., and Talbot, N.J. (1999). Identification of pathogenicity mutants of the rice blast fungus *Magnaporthe grisea* by insertional mutagenesis. Mol. Plant Microbe Interact. **12,** 129–142.

Both, M., Eckert, S.E., Csukai, M., Mueller, E., Dimopoulos, G., and Spanu, P.D. (2005). Transcript profiles of *Blumeria graminis* development during infection reveal a cluster of genes that are potential virulence determinants. Mol. Plant Microbe Interact. **18,** 125–133.

Bowyer, P., Mueller, E., and Lucas, J. (2000). Use of isocitrate lyase promoter-GFP fusion to monitor carbon metabolism of the plant pathogen *Tapesia yallundae* during infection in wheat. Mol. Plant Microbe Interact. **1,** 253–262.

Carver, T.L.W., Kunoh, H., Thomas, B.J., and Nicholson, R.L. (1999). Release and visualization of the extracellular matrix of conidia of *Blumeria graminis*. Mycol. Res. **103,** 547–560.

Chaure, P., Gurr, S.J., and Spanu, P. (2000). Stable transformation of *Erysiphe graminis*, an obligate biotrophic pathogen of barley. Nat. Biotechnol. **18,** 205–207.

Chomczynsky, P., and Sacchi, N. (1987). Single-step method of RNA isolation by acid guanidium isothiocyanate phenol chloroform extraction. Anal. Biochem. **162,** 156–159.

Clark, J.I.M., and Hall, J.L. (1998). Solute transport into healthy and powdery mildew-infected leaves of pea and uptake by powdery mildew mycelium. New Phytol. **140,** 261–269.

Cummings, C.A., Brinig, M.M., Lepp, P.W., van de Pas, S., and Relman, D.A. (2004). *Bordetella* species are distinguished by patterns of substantial gene loss and host adaptation. J. Bacteriol. **186,** 1484–1492.

Czembor, J.H. (2002). Resistance to powdery mildew in selections from Moroccan barley land races. Euphytica **125,** 397–409.

Eckert, S.E., Both, M., DeBrujin, A., Mueller, E., and Spanu, P.D. (2001). Sequence analysis and expression studies of *Erysiphe graminis* cDNAs from epiphytic mycelium. Fungal Genet. Newsl. **48,** 95.

Francis, S.A., Dewey, F.M., and Gurr, S.J. (1996). The role of cutinase in germling development and infection by *Erysiphe graminis* f. sp. *hordei*. Physiol. Mol. Plant Pathol. **49,** 201–211.

Frank, A.C., Amiri, H., and Andersson, S.G.E. (2002). Genome deterioration: Loss of repeated sequences and accumulation of junk DNA. Genetica **115,** 1–12.

Gardner, M.J., et al. (2002). Genome sequence of the human malaria parasite *Plasmodium falciparum*. Nature **419,** 498–511.

Giles, P.F., Soanes, D.M., and Talbot, N.J. (2003). A relational database for the discovery of genes encoding amino acid biosynthetic enzymes in pathogenic fungi. Comp. Funct. Genomics **4,** 4–15.

Giovanelli, J., Mudd, S.H., and Datko, A.H. (1985). Quantitative analysis of pathways of methionine metabolism and their regulation in *Lemna*. Plant Physiol. **78,** 555–560.

Ihmels, J., Levy, R., and Barkai, N. (2004). Principles of transcriptional control in the metabolic network of *Saccharomyces cerevisiae*. Nat. Biotechnol. **22,** 86–92.

Jennings, D.H. (1995). The Physiology of Fungal Nutrition. (Cambridge, UK: Cambridge University Press).

Kanehisa, M., Goto, S., Kawashima, S., Okuno, Y., and Hattori, M. (2004). The KEGG resource for deciphering the genome. Nucleic Acids Res. **32,** D277–D280.

Kinane, J., Dalvin, S., Bindslev, L., Hall, A., Gurr, S., and Oliver, R. (2000). Evidence that the cAMP pathway controls emergence of both primary and appressorial germ tubes of barley powdery mildew. Mol. Plant Microbe Interact. **13,** 494–502.

Klinkner, A.M., Bugelski, P.J., Waites, C.R., Louden, C., Hart, T.K., and Kerns, W.D. (1997). A novel technique for mapping the lipid composition of atherosclerotic fatty streaks by en face fluorescence microscopy. J. Histochem. Cytochem. **45,** 743–753.

McKeen, W.E. (1970). Lipid in Erysiphe graminis hordei and its possible role during germination. Can. J. Microbiol. **16,** 1041–1044.

Nielsen, K.A., Nicholson, R.L., Carver, T.L.W., Kunoh, H., and Oliver, R.P. (2000). First touch: An immediate response to surface recognition in conidia of *Blumeria graminis*. Physiol. Mol. Plant Pathol. **56,** 63–70.

Palmer, C.L., and Skinner, W. (2002). *Mycosphaerella graminicola*: Latent infection, crop devastation and genomics. Mol. Plant Pathol. **3,** 63–70.

Pryce-Jones, E., Carver, T., and Gurr, S.J. (1999). The roles of cellulase enzymes and mechanical force in host penetration by *Erysiphe graminis* f. sp. *hordei*. Physiol. Mol. Plant Pathol. **55,** 175–182.

Rohel, E.A., Payne, A.C., Fraaije, B.A., and Hollomon, D.W. (2001). Exploring infection of wheat and carbohydrate metabolism in *Mycosphaerella graminicola* transformants with differentially regulated green fluorescent protein expression. Mol. Plant Microbe Interact. **14,** 156–163.

Sambrook, J., Fritsch, E.F., and Maniatis, T. (1987). Molecular Cloning: A Laboratory Manual. (Cold Spring Harbor, NY: Cold Spring Harbor Laboratory Press).

Soanes, D.M., Skinner, W., Keon, J., Hargreaves, J., and Talbot, N.J. (2002). Genomics of phytopathogenic fungi and the development of bioinformatic resources. Mol. Plant Microbe Interact. **15,** 421–427.

Sokal, R.R., and Rohlf, F.J. (1981). Biometry. (New York: W.H. Freeman).

Solomon, P.S., Nielsen, P.S., Clark, A.J., and Oliver, R.P. (2000). Methionine synthase, a gene required for methionine synthesis, is expressed in planta by *Cladosporium fulvum*. Mol. Plant Pathol. **1,** 315–323.

Sutton, P.N., Henry, M.J., and Hall, J.L. (1999). Glucose, and not sucrose, is transported from wheat to wheat powdery mildew. Planta **208,** 426–430.

Talbot, N.J. (2003). On the trail of a cereal killer: Exploring the biology of *Magnaporthe grisea*. Annu. Rev. Microbiol. **57,** 177–202.

Thines, E., Weber, R.W., and Talbot, N.J. (2000). MAP kinase and protein kinase A-dependent mobilization of triacylglycerol and glycogen during appressorium turgor generation by *Magnaporthe grisea*. Plant Cell **12,** 1703–1718.

Thomas, S.W., Glaring, M.A., Rasmussen, S.W., Kinane, J.T., and Oliver, R.P. (2002). Transcript profiling in the barley mildew pathogen *Blumeria graminis* by serial analysis of gene expression (SAGE). Mol. Plant Microbe Interact. **15,** 847–856.

Thomas, S.W., Rasmussen, S.W., Glaring, M.A., Rouster, J.A., Christiansen, S.K., and Oliver, R.P. (2001). Gene identification in the obligate fungal pathogen *Blumeria graminis* by expressed sequence tag analysis. Fungal Genet. Biol. **33,** 195–211.

Thomma, B.P.H.J., van Esse, H.P., Crous, P.W., and de Wit, P.J.G.M. (2005). *Cladosporium fulvum* (syn. *Passalora fulva*), a highly specialized plant pathogen as a model for functional studies on plant pathogenic *Mycosphaerellaceae*. Mol. Plant Pathol. **6,** in press.

Tsuji, G., Fujii, S., Tsuge, S., Shiraishi, T., and Kubo, Y. (2003). The *Colletotrichum lagenarium* Ste12-like gene CST1 is essential for appressorium penetration. Mol. Plant Microbe Interact. **16,** 315–325.

Weber, R., Wakeley, G., and Pitt, D. (1999). Histochemical and ultrastructural characterization of vacuoles and spherosomes as components of the lytic system in hyphae of the fungus *Botrytis cinerea*. Histochem. J. **31,** 293–301.

Weber, R.W., Wakley, G.E., Thines, E., and Talbot, N.J. (2001). The vacuole as central element of the lytic system and sink for lipid droplets in maturing appressoria of *Magnaporthe grisea*. Protoplasma **216,** 101–112.

Weber, R.W.S., and Davoli, P. (2002). Autophagocytosis of carotenoid-rich lipid droplets into vacuoles during aeciospore ageing in *Puccinia distincta*. New Phytol. **154,** 471–479.

Wright, A.J., Thomas, B.J., and Carver, T.L.W. (2002). Early adhesion of *Blumeria graminis* to plant and artificial surfaces demonstrated by centrifugation. Physiol. Mol. Plant Pathol. **61,** 217–226.